AIAA JOURNAL
Vol. 44, No. 11, November 2006

Robustness of Acoustic Analogies for Predicting Mixing-Layer Noise

Arnab Samanta,* Jonathan B. Freund,† and Mingjun Wei‡
University of Illinois at Urbana–Champaign, Urbana, Illinois 61801
and
Sanjiva K. Lele§
Stanford University, Stanford, California, 94305

DOI: 10.2514/1.22186

Acoustic analogies for the prediction of flow noise are exact rearrangements of the flow equations $\mathcal{N}(\vec{q}) = 0$ into a nominal sound source $\mathcal{S}(\vec{q})$ and sound propagation operator $\mathcal{L}$ such that $\mathcal{L}\vec{q} = S(\vec{q})$. In practice, the sound source is typically modeled and the propagation operator inverted to make predictions. Because the rearrangement is exact, any sufficiently accurate model of the source will yield the correct sound, and so other factors must determine the merits of any particular formulation. Using data from a two-dimensional mixing-layer direct numerical simulation, we evaluate the robustness of several formulations to different errors intentionally introduced into the source. The motivation is that because $\mathcal{S}$ cannot be perfectly modeled, analogies that are less sensitive to errors in $\mathcal{S}$ are preferable. Our assessment is made within the framework of Goldstein's generalized acoustic analogy. A uniform base flow yields a Lighthill-like analogy, which we evaluate against a formulation in which the base flow is the actual mean flow of the direct numerical simulation and also against a globally parallel base flow that gives a Lilley-like analogy. The more complex mean-flow formulations are found to be significantly more robust to errors in the energetic turbulent fluctuations, but the advantage is less clear when errors are introduced at smaller scales.

Nomenclature

a_i	=	eigenfunction time coefficients
a_∞	=	ambient speed of sound
e_{ij}, η_j	=	source terms defined in (5)
h	=	enthalpy
$\mathcal{L}$	=	propagation operator
M_1, M_2	=	Mach numbers of the mixing layer
$\mathcal{N}$	=	compressible flow operator
N_t	=	number of eigenmodes
p	=	pressure
p_e	=	modified pressure defined in (4)
$\vec{q}$	=	flow field
$\mathcal{S}$	=	nominal noise source
t	=	time
T_{ij}, H_{ij}, H_0	=	source terms defined in Sec. II
u_i	=	modified flow velocity defined in (4)
v_i	=	flow velocity
$V_{1,2}$	=	mixing-layer velocity corresponding to $M_{1,2}$
y_p	=	perturbation at mixing-layer centerline
α	=	directivity (downstream is $\alpha = 0$)
γ	=	specific heat ratio
δ	=	vorticity thickness at inflow boundary
λ	=	wavelength
ρ	=	fluid density
τ_{ij}	=	stress tensor defined in (3)
ψ_i	=	empirical eigenfunctions (POD modes)
ω	=	angular frequency

Superscripts

$'$	=	perturbed quantity
$-$	=	time-averaged quantity
$\sim$	=	Favre averaged quantity
$\wedge$	=	filtered quantity

Received 2 January 2006; revision received 20 April 2006; accepted for publication 26 May 2006.

*Research Assistant, Department of Theoretical and Applied Mechanics. Student Member AIAA.

†Associate Professor, Department of Theoretical and Applied Mechanics. Senior Member AIAA.

‡Research Assistant, Department of Theoretical and Applied Mechanics; currently Postdoctoral Fellow, Princeton University, Princeton, NJ.

§Professor, Departments of Mechanical Engineering and Aeronautics & Astronautics. Senior Member AIAA.

I. Introduction

MOST approaches to predicting jet noise have three elements: designation of a noise source and propagation operator, modeling of the source, and solution of the radiated sound. Just as there is no clear separation of sound from the rest of the flow in nonlinear compressible turbulence, there is also no unique designation of a noise source in such a flow. Near flow Mach numbers of unity, many of the length and time scale separations common in acoustic analysis are unavailable to assist this designation. As a result, there are numerous possible choices for decomposing the flow equations, written compactly here for flow field $\vec{q}$ as $\mathcal{N}(\vec{q}) = 0$, into a nominal noise source $\mathcal{S}$ and propagation $\mathcal{L}$ operator: $\mathcal{L}\vec{q} = \mathcal{S}(\vec{q})$. This formulation is known as an acoustic analogy; the rearrangement is exact, but $\mathcal{S}(\vec{q})$ is treated analogously to an externally applied noise source. The (usually linear) wave operator $\mathcal{L}$ provides the means to compute $\vec{q}$ in the far field where it represents the radiated noise.

Lighthill [1] introduced the acoustic analogy by selecting $\mathcal{L}$ to be a homogeneous-medium scalar wave operator acting on the density perturbation ρ, but also recognized from the beginning [1] that this decomposition is in a sense artificial. Since this propagation operator $\mathcal{L}$ does not redirect sound, refraction is effectively lumped into $\mathcal{S}$ and is thus indistinguishable from a true noise source. The separation of propagation and generation has troubled the aeroacoustic community ever since. It can be argued that choices of $\mathcal{L}$ and $\mathcal{S}$ that better separate true sources from propagation provide a firmer platform upon which to begin modeling the sources. The linearized Lilley equation [2,3] is a common choice for attempting to accomplish this separation. In this formulation, a parallel base flow and any refraction it causes is explicit in $\mathcal{L}$. However, it does not

provide any obvious simplification of the source $\mathcal{S}$ aside from possibly localizing it, which might in some sense make it easier to model. Nevertheless, it still leaves complex combinations of terms which must be modeled in making predictions. Since there is no obvious simplification that comes about by incorporating more propagation physics into $\mathcal{L}$, it can therefore also be argued that the Lighthill approach is no worse off than such a more sophisticated approach. Since the Lighthill analogy, like any acoustic analogy, is exact, an accurate representation of the source provides the correct sound despite the multiple physical effects grouped into it. This makes it difficult to support any one formulation as being preferable to any other.

In this paper, we take a new approach and empirically assess the *robustness* of different acoustic analogies to errors in their respective noise sources ($\mathcal{S}$). Since $\mathcal{S}$ will never be modeled exactly in practice, we explore whether some $\mathcal{L}\vec{q} = \mathcal{S}(\vec{q})$ decompositions are more robust to errors than others. To make our assessment, we employ Goldstein's recently developed generalized acoustic analogy [4], which provides a single clear framework for a family of consistent $\mathcal{L}$'s and $\mathcal{S}$'s. The formulation is described in Sec. II. The noise source data are taken from a direct numerical simulation (DNS), also described in this section. Robustness is assessed by comparing predictions when errors are purposely introduced into the source as described in Sec. III. Specifically, we consider formulations built on a homogeneous-medium wave equation as in Lighthill's formulation, a parallel base flow as in Lilley's equation, and a spreading mean-flow taken from the DNS, which is now straightforward in Goldstein's formulation. We also evaluate a locally parallel flow approximation for $\mathcal{L}$ and $\mathcal{S}$, which is, however, not a formally constructed acoustic analogy because it is not an exact decomposition. The large errors that we observe for the Lighthill-like formulation are explained in Sec. IV with a simple model.

II. Preliminaries

A. Formulation

The propagation operator in Goldstein's [4] generalized acoustic analogy is similar to linearized Euler equations:

$$\bar{\rho}\frac{\bar{D}}{Dt}\frac{\rho'}{\bar{\rho}} + \frac{\partial \bar{\rho} u_j'}{\partial x_j} = 0 \tag{1a}$$

$$\bar{\rho}\left(\frac{\bar{D}u_i'}{Dt} + u_j'\frac{\partial \tilde{v}_i}{\partial x_j}\right) + \frac{\partial p_e'}{\partial x_i} - \frac{\rho'}{\bar{\rho}}\frac{\partial \tilde{\tau}_{ij}}{\partial x_j} = \frac{\partial}{\partial x_j}(e_{ij}' - \tilde{e}_{ij}) \tag{1b}$$

$$\frac{1}{\gamma - 1}\left(\frac{\bar{D}p_e'}{Dt} + \gamma p_e'\frac{\partial \tilde{v}_j}{\partial x_j} + \gamma\frac{\partial \bar{p}u_j'}{\partial x_j}\right) - u_i'\frac{\partial \tilde{\tau}_{ij}}{\partial x_j} = \frac{\partial}{\partial x_j}(\eta_j' - \tilde{\eta}_j) + (e_{ij}' - \tilde{e}_{ij})\frac{\partial \tilde{v}_i}{\partial x_j} \tag{1c}$$

where

$$\frac{\bar{D}}{Dt} \equiv \frac{\partial}{\partial t} + \tilde{v}_j\frac{\partial}{\partial x_j} \tag{2}$$

and

$$\tilde{\tau}_{ij} \equiv \delta_{ij}\bar{p} - \tilde{T}_{ij} - \tilde{\sigma}_{ij} \tag{3}$$

The base flow that defines the specific analogy has density $\bar{\rho}$, pressure $\bar{p}$, and velocity $\tilde{v}_i$ and satisfies exact equations with sources $\tilde{T}_{ij}$, $\tilde{H}_{ij}$, and $\tilde{H}_0$ [4]. For example, the momentum equations for a time-averaged base flow has Reynolds stresses as sources. Perturbations from this base flow are ρ', p', and v_i'. To put (1) into its relatively clean form, new dependent variables were constructed from nonlinear combinations of the primitive variables as

$$p_e' \equiv p' + \frac{\gamma - 1}{2}\rho v_i v_i + (\gamma - 1)\tilde{H}_0 \quad \text{and} \quad u_i' \equiv \rho\frac{v_i'}{\bar{\rho}} \tag{4}$$

which become $p_e' = p'$ and $u_i = v_i$ in the far field or linear acoustic limit.

The source terms on the right-hand side of (1b) and (1c) are the $\mathcal{S}$ discussed in Sec. I. They are

$$e_{ij}' \equiv -\rho v_i' v_j' + \frac{\gamma - 1}{2}\delta_{ij}\rho v_k' v_k' + \sigma_{ij}' \tag{5a}$$

$$\tilde{e}_{ij} \equiv \tilde{T}_{ij} - \delta_{ij}(\gamma - 1)\tilde{H}_0 \tag{5b}$$

$$\eta_i' \equiv -\rho v_i' h_0' - \theta_i' + \sigma_{ij} v_j' \tag{5c}$$

$$\tilde{\eta}_i \equiv \tilde{H}_i - \tilde{T}_{ij}\tilde{v}_j \tag{5d}$$

where σ is a viscous stress tensor and θ is a diffusive heat flux. The enthalpy h_0' is $h_0' \equiv h' + v_i' v_i'/2$, where h' is a perturbation to the base flow thermodynamic enthalpy.

We consider three base flow choices in this paper. The first is a uniform flow,

$$\bar{\rho} = \rho_\infty, \qquad \bar{p} = p_\infty, \qquad \tilde{v}_1 = V_1, \quad \text{and} \quad \tilde{v}_2 = \tilde{v}_3 = 0 \tag{6}$$

which gives a Lighthill-like formulation for a uniform velocity homogeneous medium. We take V_1 to be the velocity of the slow speed side of the mixing layer that we study. In this case, $\tilde{T}_{ij}$, $\tilde{H}_{ij}$, and $\tilde{H}_0$ are all zero, and so the sources are

$$e_{ij}' - \tilde{e}_{ij} = -\rho v_i' v_j' + \frac{\gamma - 1}{2}\delta_{ij}\rho v_k' v_k' \tag{7}$$

and

$$\eta_i' - \tilde{\eta}_i = -\rho v_i' h_0' \tag{8}$$

where we have omitted molecular diffusion terms as we do throughout in the discussion and in the numerical calculations. Viscous effects have an insignificant effect on the sound generated by flows of this type. In this case, perturbations are from the uniform flow (6), not the mean flow.

In the second case, a globally parallel base flow, which is an exact solution of the base flow equations with the source terms equal to zero (i.e., Euler's equations), is used with

$$\bar{\rho} = \bar{\rho}(x_2), \qquad \bar{p} = p_\infty, \qquad \tilde{v}_1 = V_1(x_2), \quad \text{and} \quad \tilde{v}_2 = \tilde{v}_3 = 0 \tag{9}$$

The base flow $\bar{\rho}$ and V_1 were taken from the time-averaged DNS at the midpoint of the downstream domain in x_1. This gives the same source as (7) and (8), but now the fluctuations are measured relative to the parallel base flow.

For the final acoustic analogy case, we took the time-averaged DNS flow to be the base flow. In this case, an overbar ($\bar{\cdot}$) indicates a time average with corresponding Favre average ($\tilde{\cdot}$). Thus we have noise sources

$$e_{ij}' - \tilde{e}_{ij} = -\rho v_i' v_j' + \overline{\rho v_i' v_j'} + \frac{\gamma - 1}{2}\delta_{ij}(\rho v_k' v_k' - \overline{\rho v_k' v_k'}) \tag{10}$$

and

$$\eta_i' - \tilde{\eta}_i = -\rho v_i' h_0' + \overline{\rho v_i' h_0'} \tag{11}$$

both of which have zero mean.

The above formulations are exact, or at least could be were viscous effects included. We also consider an approximation which follows directly from the exact mean-flow formulation by assuming a locally parallel flow. In this case, only the transverse derivatives (∂_{x_2}) of time-averaged quantities in $\mathcal{L}$ and $\mathcal{S}$ are retained in (1) and (5). The resulting $\mathcal{L}$ is the same as proposed by Tam and Auriault [5], but the

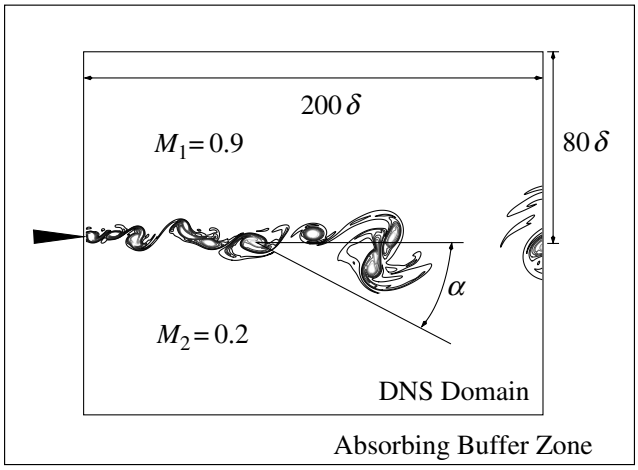

Fig. 1 Schematic of the computational domain with vorticity magnitude showing the mixing layer. The angle α indicates the measured directivity direction (see text), with the radius vector centered at (50δ, 0).

source we calculate is an approximation of the exact $\mathcal{S}$. For convenience we discuss it simply as a separate case along with the formal acoustic analogies in the following.

B. DNS Data and Acoustic Analogy Solution

The DNS data used is that of a two-dimensional mixing-layer flow between Mach 0.9 and Mach 0.2 free streams at the same temperature. An instantaneous vorticity field is visualized in Fig. 1, which also shows that the physical domain of the simulation extends from $x = 0$ to 200δ downstream and from $y = -80$ to 80δ in the transverse direction, where δ is the vorticity thickness at the inflow boundary. The Reynolds number based on the velocity difference and δ is 500. Full details of the numerical method and simulation procedure, including the specifics of the inflow excitation, are provided elsewhere [6]. The only difference here is that the present x domain and total simulation time have both been doubled while maintaining the same mesh resolution.

Flow fields were saved every four numerical time steps during simulation. All necessary averages, correlations, and source terms needed for the acoustic analogies were computed directly from this stored DNS data. Equation (1) was solved directly on the same mesh as the direct numerical simulation using a similar algorithm with the same numerical time step as the DNS. Spatial derivatives were computed using a fourth-order seven-point explicit coefficient-optimized finite-difference scheme [7] in both the directions. A fourth-order Runge–Kutta algorithm was used for time advancement. The source was interpolated in time as necessary using a cubic spline with 16 knots. For both the DNS data and the analogy solutions, the sound was extrapolated into the far field by a semianalytic solution of the wave equation in the same manner as by Freund [8]. The full details of this procedure and its validation are documented elsewhere [6,9].

III. Robustness to Source Errors

As discussed in Sec. I, the primary objective of this work is to assess the robustness of the noise predictions to errors in the nominal noise source, and so we must somehow specify these errors. Here, we only consider errors that arise from omitting part of the flow solution from the source computation. In practice, this error might be the missing small-scale turbulence in a large-eddy simulation or due to imperfect modeling of the larger turbulent scales in, say, a parabolized Navier–Stokes model of a mixing layer or jet [10,11], but we make no attempt to rigorously represent any particular source of error.

A. Errors Introduced Via Normal Mode Decomposition

In this first of the two error methods that we consider, the flow was simply decomposed into empirical Karhunen-Loeve (KL) eigenfunctions $\vec{\psi}_i(\mathbf{x})$ [12], also commonly called proper orthogonal decomposition (POD) modes, with time coefficients $a_i(t)$ such that the flow $\vec{q}$ is reconstructed as

$$\vec{q}(\mathbf{x}, t) = \sum_{i=1}^{N_t} a_i(t)\vec{\psi}_i(\mathbf{x}) \tag{12}$$

In this study, the kinetic energy norm

$$E = \int_{\mathcal{V}} \rho u_i u_i d\mathcal{V} \tag{13}$$

defines the eigenfunctions in the usual way. Subsets of these modes were then used to reconstruct the flow and calculate approximations to e_{ij} and η_i defined in (5). To compute $\vec{\psi}_i$, we used the method of snapshots [13] with 558 data fields sampled at regular intervals from the 3907 available fields stored from the simulation.

The fraction of the kinetic energy contained by each KL modes is shown in Fig. 2. Figure 3 shows the spatial form of the y-velocity component for the $i = 1$ and $i = 128$ modes, their corresponding time coefficients $a_i(t)$ and also their time spectra. Clearly, lower-order modes are of larger scale and lower frequency. Instability wavelike modes, such as the $i = 1$ one here have also been detected even in high-Reynolds-number turbulent jets [14]. We use these modes to form two types of erroneous reconstructions for our robustness assessment. The first is simple truncation of the reconstruction series in (12) at N_t, where $N_t < 558$. Specifically, we consider cases with $N_t = 32$ and 128, which include 91.3, and 99.3% of the energy, respectively. The other form of error is introduced by changing the contribution of one or two of the lowest-order modes. We consider two such cases: $a'_1(t) = 0.5a_1(t)$ and $a'_{1,2}(t) = 0.5a_{1,2}(t)$. In the second case, both the lowest-order modes are halved.

Table 1 describes the five cases for which we present results. Sound spectra for all these cases are presented in Figs. 4 and 5 at directivity angles $\alpha = 50$ and 130°, respectively, where α is measured from the downstream x axis toward the slow speed stream (see Fig. 1). The spectra at $\alpha = 90°$ show a behavior that is qualitatively intermediate between these two cases. At all angles, the full source case A produces a good match with the DNS directivity, as it should if implemented correctly. The differences are believed to be due to boundary conditions and other numerical errors and are much smaller than the disagreement we will see in the other cases. At the highest frequencies all analogies show a similar error, all starting at about the same frequency. We take this as a lower bound for the

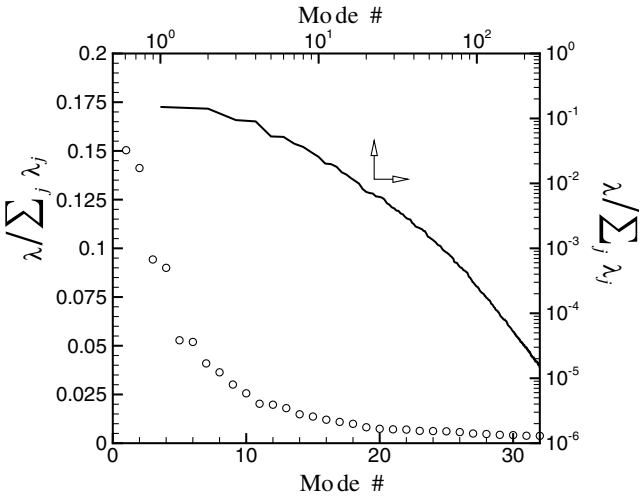

Fig. 2 Fraction of kinetic energy defined by (13) of each mode. The solid line corresponds to the top and right logarithmic axes.

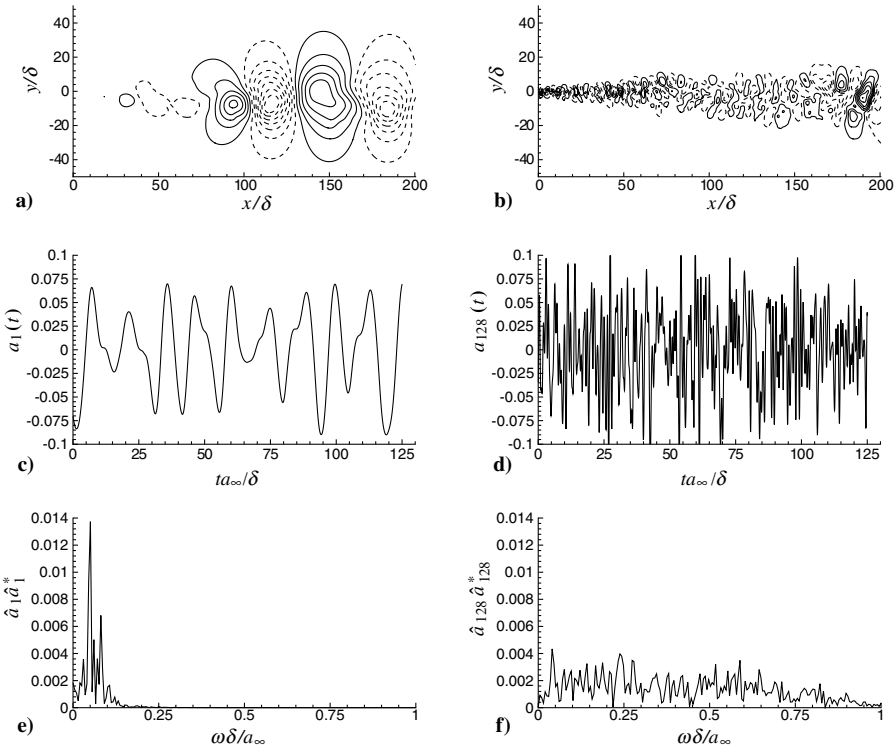

Fig. 3 Empirical eigenfunctions: mode shapes a),b), time coefficients c),d), and spectra e),f) for modes 1 a), c), e) and 128 b), d), f). In a) and b) negative contours are dashed.

range of intensities over which we can make meaningful comparisons and assume that the subsequent calculations share this threshold. Note that in all these plots we do not cut off the spectra.

Despite representing nearly all the kinetic energy of the mixing layer, retaining 128 modes (case B) for all the formulations produces significant erroneous noise in the higher frequencies. The mean-flow analogy is somewhat closer to the DNS at higher frequencies in the $\alpha = 50°$ case while the Lighthill-like model is somewhat closer for the intermediate range of frequencies at both the angles studied. The globally parallel flow analogy behaves similar to the mean-flow analogy, except at lower frequencies where it shows relatively more error, though all formulations match quite well at the lowest frequencies. Retaining fewer modes as in case C leads to similar errors, but with the lower frequencies affected more significantly, which is expected because lower-order modes have lower frequency content.

A much more significant difference is observed when we disrupt the lower frequency, larger-scale structures by altering the lowest-order POD mode in case D. Since all the remaining modes were exactly retained, we expect the same behavior as the full source case (case A) at higher frequencies, but at $\alpha = 130°$ we also now see large over prediction errors in the low frequencies for the uniform-flow (Lighthill) analogy. All the formulations with mean shear included in $\mathcal{L}$ do not seem to have this extreme sensitivity. The errors we see at $\alpha = 50°$ are relatively minor compared with higher angles. Clearly, the complexity introduced by better distinguishing propagation from true acoustic sources appears to be worthwhile in this case, because the errors in the sound prediction are in better proportion to the errors (by a kinetic energy measure) introduced into the noise source. Similar exaggerated errors are also observed if we disrupt the third mode (a_3), but they appear, as expected, at somewhat higher frequencies. However, the pronounced error in the uniform base flow case seems to decrease when we disrupt both the two lowest-order modes in case E. This behavior is explained in Sec. IV.

Table 1 Cases presented

Case	Energy retained	Description
A	100.0%	Full source information
B	99.3%	128 modes
C	91.3%	32 modes
D	92.5%	$a'_1 = a_1/2$
E	85.5%	$a'_{1,2} = a_{1,2}/2$

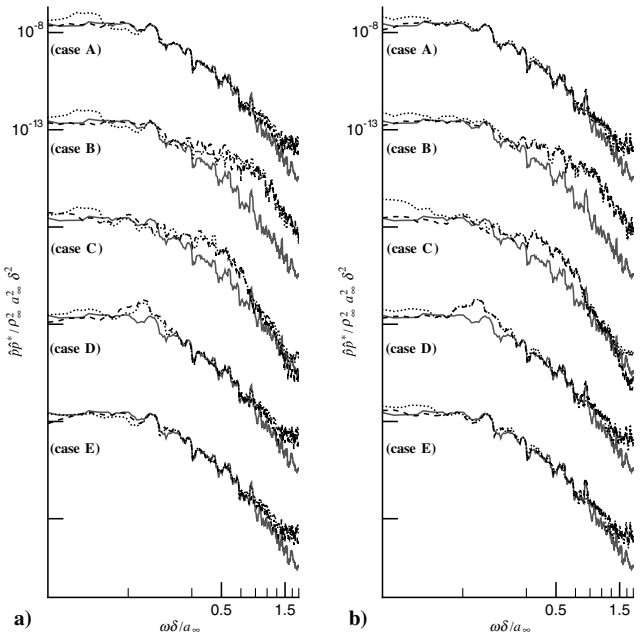

Fig. 4 Sound pressure spectra at $\alpha = 50°$: a) solid line DNS, dashed line DNS-mean base flow analogy, and dotted line uniform base flow analogy; and b) solid line DNS, dashed line globally parallel base flow analogy, and dotted line locally parallel flow approximation. In both, A through E labels show cases A through E as defined in Table 1.

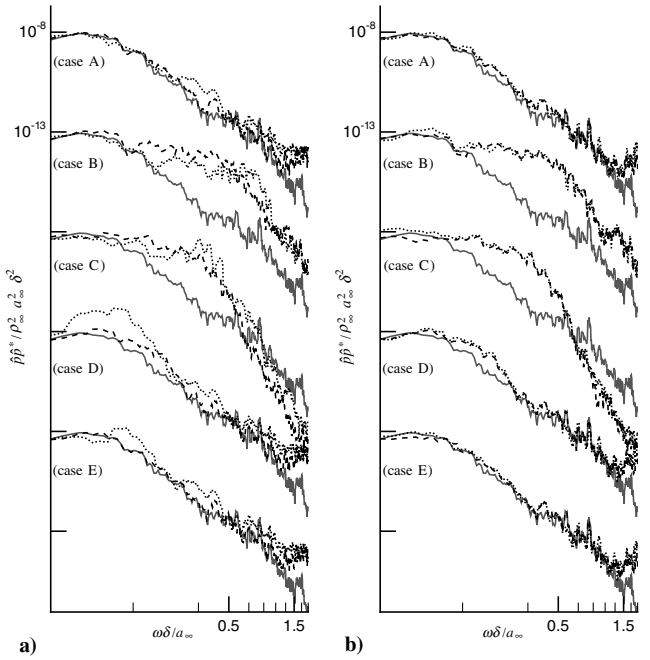

Fig. 5 Same as Fig. 4 at $\alpha = 130°$.

The changes in the radiation pattern can be seen more clearly with sound-field visualizations. Figure 6a shows the sound field for the DNS, which is well matched by all the analogies for the full source. The truncation of the POD modes beyond the first 128 modes creates small-scale, high-frequency noise of the type we see in Fig. 6b, which is expected and is insensitive to the analogy formulations. More notable changes are observed for case D of Table 1. The $a_1/2$ case is a significant disruption, and the sound is altered for all the analogies, though the effect is relatively minor for the DNS-mean-flow analogy's sound field visualized in Fig. 6c. However, for the Lighthill-like analogy, there is a new and very strong upstream radiation [see Fig. 6d], which is absent in the other cases. Its pattern is reminiscent of jet screech, though this flow is subsonic. This strong upstream sensitivity is, however, absent for case E.

B. Filtering Errors

We also introduced error by applying a spatial filter directly to the DNS data. This filtered data was then used to compute the averages, correlations, and sources as necessary for each analogy. The filter had a transfer function $T(\lambda) = 0.5$ for spatial wavelength of $\lambda = 15.7\delta$. Its full details are provided in the Appendix. The far-field sound spectra in this case (see Fig. 7) shows somewhat greater errors for the uniform base flow analogy, but not as significantly as for the $a_1/2$ cases in Sec. III.A.

IV. Discussion of Uniform Base Flow Case

As is clear from the results of Sec. III, the uniform base flow type analogy showed a pathological sensitivity to certain source errors that disrupt the large-scale structure of the flow. In Fig. 6d we saw that errors of this kind led to intense upstream propagating waves reminiscent of the feedback component of screech noise. In this section we explain this particular behavior with a simple model.

Figure 8 shows a component of the noise source for the DNS-mean base flow case and the uniform base flow case. They are notably different. The source in the uniform base flow case [Fig. 8b] has a wavy character, whereas the absence of a mean component in the DNS-mean base flow case yields only blob structures that convect downstream [Fig. 8a]. We can demonstrate that it is this wavy structure that makes the uniform base flow case particularly sensitive to a disruption of one of its low-order POD modes.

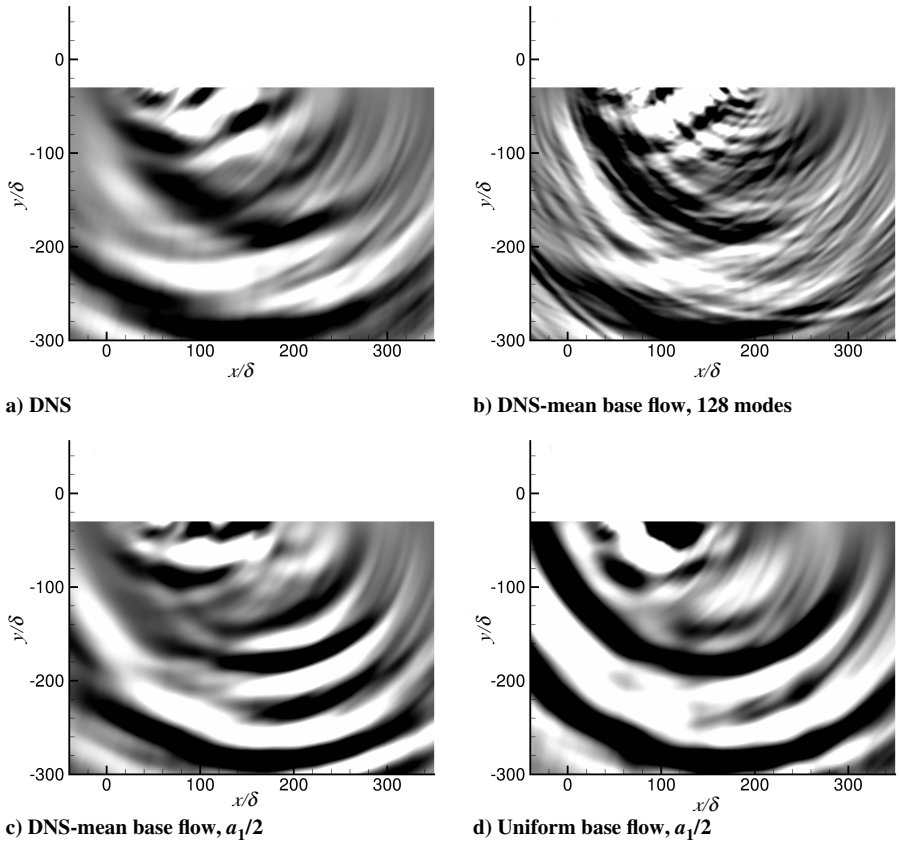

Fig. 6 Sound-field pressure visualizations: a) DNS; b) DNS-mean base flow analogy for case B; c) DNS-mean base flow analogy for case D; d) uniform base flow analogy for case D. Grey levels indicate $p'/\rho_\infty a_\infty^2$ between ± 0.002.

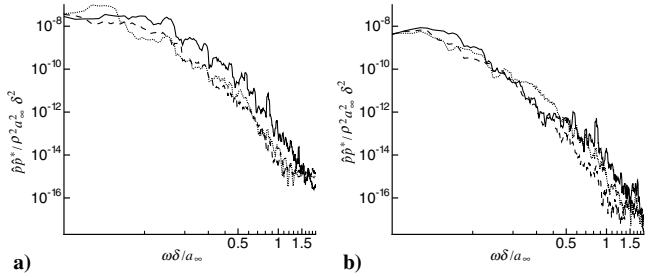

Fig. 7 Filtered sound pressure spectra at a) $\alpha = 50°$ and b) $\alpha = 130°$: solid line DNS; dashed line DNS-mean base flow analogy; dotted line uniform base flow analogy.

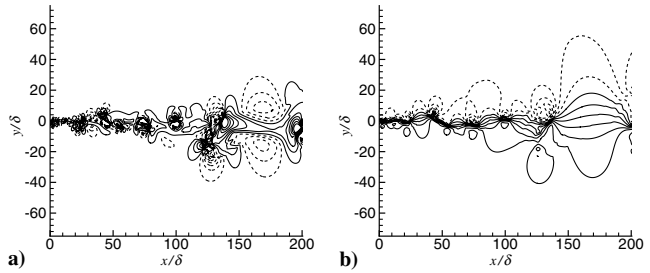

Fig. 8 Noise source components for a) the DNS-mean base flow analogy, and b) the uniform base flow analogy. In a) contour levels indicate $\rho v_1' v_1'$ between ± 0.05, with the negative contours dashed. In b) contour levels are between $0 < \rho v_1' v_1' < 0.7$, with dashed lines showing the upper half of that contour range.

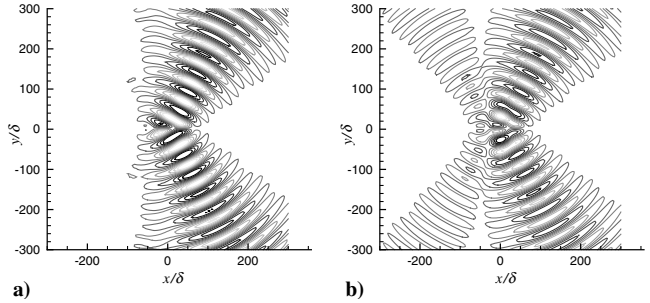

Fig. 9 Solutions of (17) for the model flow: a) full source and b) source with the error $a_1' = a_1/2$.

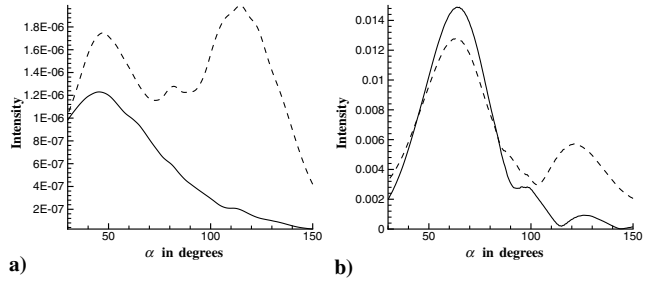

Fig. 10 Sound-field directivity at a radius of 300δ: a) numerical simulation (case D of Table 1), b) the model employed. In each frame solid line indicates full source and dashed line indicates source with the error $a_1' = a_1/2$.

We assume that the two lowest-order modes give a convected harmonic wave modulated by a Gaussian envelop,

$$y_p = e^{-\eta x^2}[a_1(t)\cos kx + a_2(t)\sin kx] \tag{14}$$

with coefficients

$$a_1(t) = -\sin\omega t \quad \text{and} \quad a_2(t) = \cos\omega t \tag{15}$$

This form is supported by the more detailed POD analysis of this type of flow [6]. Taking

$$u_1 = \tfrac{1}{2}(M_1 - M_2)\{\tanh[\xi(y - y_p)] + 1\} + M_2 \tag{16}$$

and having y_p vary as in (14) gives the flow a wavy character with an undulating shear layer centerline similar to that seen in Fig. 8b. We then solve

$$\left(\nabla^2 - \frac{1}{a_\infty^2}\frac{\partial^2}{\partial t^2}\right)\rho(\mathbf{x}, t) = -\frac{1}{a_\infty^2}\frac{\partial^2 \rho u_1 u_1}{\partial x_1 \partial x_1} \tag{17}$$

which is essentially Lighthill's equation with only the $\rho u_1 u_1$ component of the source. Parameters $M_1 = 0.9$, $M_2 = 0.2$, $\eta = 0.00035$, and $\xi = 0.1$ were selected based on the DNS flow. The resulting sound field is downstream directed, which is visualized in Fig. 9a. However, taking $a_1' = a_1/2$ yields the sound field shown in Fig. 9b. There is now a distinct upstream component similar to that seen in Fig. 6d. The sound in this direction is increased by over 10 decibels. This is also seen in the sound-field directivity of Fig. 10. Without the mean-flow component in the source, this extreme sensitivity is absent. The upstream radiation also of course vanishes on taking $a_{1,2}' = a_{1,2}/2$, similar to what was observed for case E of Table 1. The particular behavior we observe is probably specific to our flow, but the potential for this type of behavior is expected to be much more general.

V. Further Discussion and Conclusions

There are two ways that we can anticipate acoustic analogies being used in a time dependent formulation of the type tested here. The first would be in conjunction with a large-eddy simulation or similar accelerated solution of the flow equations which represents only the larger, more energetic scales of the flow. The analogy in this case might be used in conjunction with a sub-grid-scale source model to predict the noise from the missing scales [15]. This application best corresponds to the error models in which we truncated the sum in (12) at finite N_t, omitting for the most part smaller scale unsteadiness.

The second type of time dependent acoustic analogy application we envision would be in conjunction with a model for the largest scales of a turbulent flow, such as a solution of the parabolized Navier–Stokes equations [10,11] or a dynamic model constructed by projecting POD modes onto the governing equations. Such a representation would, of course, contain some errors, which we modeled by altering the time coefficient of the lowest-order modes.

The results above suggest that neither formulation has a clear advantage for modeling the contribution of the missing small scales to the higher frequencies in the noise spectrum, though this might, of course, depend upon the specifics of the particular formulation used. In this study we have a rather stringent accuracy demand which assesses agreement over ~50 decibels decay in the spectra. The noise spectrum of turbulent flow typically decays more slowly with frequency than seen here and therefore might potentially show different results. However, analogy formulations with the dominant refraction included in $\mathcal{L}$ do seem to be preferable in the second case, where the Lighthill-like formulation shows significant errors. A simple model demonstrates that it is specifically the wavy character of the source due to the inclusion of the mean-flow in it which gives rise to this sensitivity. Further study of the robustness of statistical noise models with more complex and heated jets is warranted. We can anticipate that these more complex flows might better delineate the merits of the various formulations.

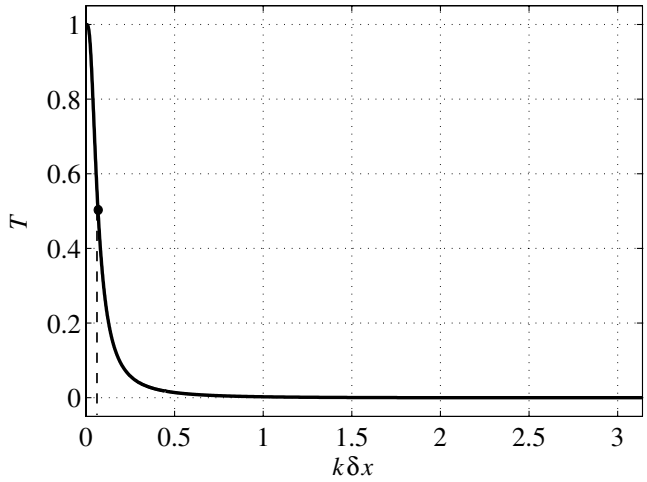

Fig. A1 Transfer function of the low pass filter used.

Aside from their complexity, another purported disadvantage of the mean-flow analogy is that the resulting linearized Euler equations support instability wave homogeneous solutions, which have the potential to overwhelm the solution. However, no special treatment was required in the present case. The homogeneous solution is excited, but does not degrade the acoustic predictions.

Appendix

The filter used in Sec. III.B has the form

$$w_2\hat{f}_{i-2} + w_1\hat{f}_{i-1} + \hat{f}_i + w_1\hat{f}_{i+1} + w_2\hat{f}_{i+2} = \sum_{j=0}^{N} \frac{c_j(f_{i-j} + f_{i+j})}{2} \tag{A1}$$

where $\hat{f}_i$ represents the filtered variable obtained from the original variable f. Coefficients were selected to maintain sixth-order accuracy which following Lele [16] provides four equations for the coefficients, leaving the c_i's expressed in terms of w_1 and w_2 for $N = 3$. The remaining two equations are obtained by requiring the transfer function of (A1)

$$T(k\Delta x) = \frac{\sum_{n=0}^{N} c_n \cos(nk\Delta x)}{1 + 2w_1\cos(k\Delta x) + 2w_2\cos(2k\Delta x)} \tag{A2}$$

to satisfy

$$T(k_1\Delta x) = s_1 \qquad T(k_2\Delta x) = s_2 \tag{A3}$$

for $0 \le k\Delta x \le \pi$. We chose $k_1\Delta x = 0.03$ and $k_2\Delta x = 0.09$ for $s_1 = 0.9$ and $s_2 = 0.35$ respectively, which result in the following filter parameters:

$$\begin{aligned} w_2 &= 0.16645 \\ w_1 &= -0.66645 \\ c_0 &= \tfrac{1}{4}(2 + 3w_1) \\ c_1 &= \tfrac{1}{16}(9 + 16w_1 + 10w_2) \\ c_2 &= \tfrac{1}{4}(w_1 + 4w_2) \\ c_3 &= \tfrac{1}{16}(6w_2 - 1) \end{aligned} \tag{A4}$$

The transfer function is shown in Fig. A1, where one-half amplitude reduction point occurs at $k\Delta x \approx 0.07$.

Acknowledgments

A. S. and J. B. F. gratefully acknowledge support from NASA. The mixing-layer DNS simulations of M. W. were supported by the Air Force Office of Scientific Research. The study was initiated during the 2004 Center for Turbulence Research summer program.

References

[1] Lighthill, M. J., "On Sound Generated Aerodynamically: I. General Theory," *Proceedings of the Royal Society of London A*, Vol. 211, March 1952, pp. 564–587.
[2] Lilley, G. M., "On the Noise from Jets," AGARD CP-131, 1974.
[3] Goldstein, M. E., *Aeroacoustics*, McGraw–Hill Book Co., New York, 1976.
[4] Goldstein, M. E., "A Generalized Acoustic Analogy," *Journal of Fluid Mechanics*, Vol. 488, Aug. 2003, pp. 315–333.
[5] Tam, C. K. W., and Auriault, L., "Jet Mixing Noise from Fine-Scale Turbulence," *AIAA Journal*, Vol. 37, No. 2, 1999, pp. 145–153.
[6] Wei, M., and Freund, J. B., "A Noise-Controlled Free Shear Flow," *Journal of Fluid Mechanics*, Vol. 546, Jan. 2006, pp. 123–152.
[7] Tam, C. K. W., and Webb, J. C., "Dispersion-Relation-Preserving Finite Difference Schemes for Computational Acoustics," *Journal of Computational Physics*, Vol. 107, No. 2, 1993, pp. 262–281.
[8] Freund, J. B., "Noise Sources in a Low-Reynolds-Number Turbulent Jet at Mach 0.9," *Journal of Fluid Mechanics*, Vol. 438, July 2001, pp. 277–305.
[9] Wei, M., "Jet Noise Control by Adjoint-Based Optimization," Ph.D. Thesis, Department of Theoretical and Applied Mechanics, University of Illinois at Urbana–Champaign, Urbana, Illinois, 2004.
[10] Bertolotti, F., and Colonius, T., "On the Noise Generated by Shear-Layer Instabilities in Turbulent Jets," AIAA Paper 2003-1062, 2003.
[11] Cheung, L., and Lele, S. K., "Acoustic Radiation from Subsonic and Supersonic Mixing Layers with Nonlinear PSE," AIAA Paper 2004-0363, 2004.
[12] Holmes, P., Lumley, J. L., and Berkooz, G., *Turbulence, Coherent Structures, Dynamical Systems and Symmetry*, Cambridge University Press, Cambridge, 1996.
[13] Sirovich, L., "Chaotic Dynamics of Coherent Structures. Parts I–III," *Quarterly of Applied Mathematics*, Vol. 45, No. 3, 1987, pp. 561–582.
[14] Suzuki, T., and Colonius, T., "Identification of Jet Instability Waves and Design of a Microphone Array," AIAA Paper 2004-2960, 2004.
[15] Bodony, D. J., and Lele, S. K., "On Using Large-Eddy Simulation for the Prediction of Noise from Cold and Heated Turbulent Jets," *Physics of Fluids*, Vol. 17, 085103, 2005.
[16] Lele, S. K., "Compact Finite Difference Schemes with Spectral-Like Resolution," *Journal of Computational Physics*, Vol. 103, No. 1, 1992, pp. 16–42.

D. Gaitonde
Associate Editor